

# Reconstructing East Asian Temperatures from 1368 to 1911 Using Historical Documents, Climate Models, and Data Assimilation

Eric Sun<sup>a</sup>, Kuan-hui Elaine Lin<sup>b</sup>, Wan-Ling Tseng<sup>c</sup>, Pao K. Wang<sup>d</sup>, Hsin-Cheng Huang<sup>a,\*</sup>

<sup>a</sup>*Institute of Statistical Science, Academia Sinica, Taiwan*

<sup>b</sup>*Graduate Institute of Sustainability Management and Environmental Education, National Taiwan Normal University, Taiwan*

<sup>c</sup>*International Degree Program in Climate Change and Sustainable Development, National Taiwan University, Taiwan*

<sup>d</sup>*Research Center for Environmental Changes, Academia Sinica, Taiwan*

---

## Abstract

We present a novel approach for reconstructing annual temperatures in East Asia from 1368 to 1911, leveraging the Reconstructed East Asian Climate Historical Encoded Series (REACHES). The lack of instrumental data during this period poses significant challenges to understanding past climate conditions. REACHES digitizes historical documents from the Ming and Qing dynasties of China, converting qualitative descriptions into a four-level ordinal temperature scale. However, these index-based data are biased toward abnormal or extreme weather phenomena, leading to data gaps that likely correspond to normal conditions. To address this bias and reconstruct historical temperatures at any point within East Asia, including locations without direct historical data, we employ a three-tiered statistical framework. First, we perform kriging to interpolate temperature data across East Asia, adopting a zero-mean assumption to handle missing information. Next, we utilize the Last Millennium Ensemble (LME) reanalysis data and apply quantile mapping to calibrate the kriged REACHES data to Celsius temperature scales. Finally, we introduce a novel Bayesian data assimilation method that integrates the kriged Celsius data with LME simulations to enhance reconstruction accuracy. We model the LME data at each geographic location using a flexible nonstationary autoregressive time series model and employ regularized maximum likelihood estimation with a fused lasso penalty. The resulting dynamic distribution serves as a prior, which is refined via Kalman filtering by incorporating the kriged Celsius REACHES data to yield posterior temperature estimates. This comprehensive integration of historical documentation, contemporary climate models, and advanced statistical methods improves the accuracy of historical temperature reconstructions and provides a crucial resource for future environmental and climate studies.

*Keywords:* Fused lasso, interval censored data, kriging, quantile mapping, uncertainty quantification

---

\*Corresponding author

*Email address:* `hchuang@stat.sinica.edu.tw` (Hsin-Cheng Huang)

## 1. Introduction

Climate change is a complex, multidimensional process with profound implications for the sustainability of our planet. Driven by the interplay between human activities and natural climatic processes, it necessitates comprehensive strategies encompassing mitigation and adaptation. An in-depth understanding of historical climate patterns and their impacts is essential for devising informed and effective strategies to safeguard future generations.

In response to this need, a research team at Academia Sinica has developed an innovative index-based historical climate database: the Reconstructed East Asian Climate Historical Encoded Series (REACHES, Wang et al., 2018). This database utilizes a wealth of Chinese historical documents from the Ming (1368–1644 CE) and Qing (1644–1912 CE) dynasties, offering a unique perspective on paleoclimate in East Asia.

Despite its rich historical context, the REACHES database has limitations in geographic and temporal coverage. The data primarily originate from sites with existing narrative records, leading to a significant reduction in data volume in earlier years and less inhabited regions. Additionally, the variables in the dataset are categorized into a limited number of classes. For temperature, there are four ordinal indices: -2 (very cold), -1 (cold), 0 (normal), and 1 (warm). This classification, influenced by the asymmetry where cold events are more frequently documented than warm ones, tends to emphasize extreme weather events and creates gaps in the records for normal weather conditions. To overcome these challenges and enhance the dataset’s utility, we devise a three-tiered statistical framework to correct these biases and enable a more comprehensive reconstruction of historical temperatures across East Asia.

In the initial phase of our methodology, we employ kriging, the best linear unbiased prediction technique, to interpolate annual temperature data for regions lacking direct records. We adopt a zero-mean assumption based on the hypothesis that areas without data generally experienced normal weather conditions (Wang et al., 2024). Additionally, we treat the index data as interval-censored to address their discontinuous nature. This approach yields a geo-

statistically smoothed surface across East Asia, providing spatially continuous temperature estimates along with associated uncertainty quantifications.

The second phase involves converting the kriged temperature data into Celsius scales using a quantile mapping technique (Cannon et al. 2015). This adjustment aligns the distribution of the kriged data from REACHES with temperature data from the Community Earth System Model Last Millennium Ensemble (LME), a comprehensive global climate model (Otto-Bliesner et al. 2016).

In the final phase, we refine the Celsius-scaled kriged data using Bayesian data assimilation techniques, treating them as derived observational proxies with inherent uncertainties. By integrating these proxies with dynamical structures derived from separately run LME model outputs and applying offline data assimilation methods (Oke et al. 2002), we significantly enhance the accuracy of our predictions. This integration merges narrative-based reconstructions with model simulations, leveraging both historical information and physical models to substantially improve the precision and reliability of historical temperature reconstructions.

To support this intricate process, our methodology incorporates a nonstationary autoregressive time series model that accommodates heterogeneities in the mean and autoregressive structures suggested by the LME model outputs. We enhance the robustness of our estimations by applying regularized maximum likelihood estimation with a fused lasso penalty (Tibshirani et al., 2004), which promotes continuity and smoothness among adjacent coefficients. An efficient coordinate descent algorithm is implemented to solve the regularized maximum likelihood estimation. Using the estimated model as a prior of true temperature states over time, we further refine the Celsius-scaled REACHES data by applying the Kalman filter and smoother.

Data assimilation has become an indispensable technique across various fields, renowned for enhancing the precision of forecasts and reconstructions by synthesizing observational data with predictions from climate models (see Kalnay 2002; Evensen 2009). Notable

methods include Kalman filters (Kalman 1960; Wang et al. 2021), variational techniques (Brousseau et al. 2011), and particle filters (Goosse et al. 2012), each contributing to the creation of comprehensive and continuous climate models and providing essential uncertainty quantifications. Despite its broad applicability, integrating sparse and heterogeneous datasets with complete climate models remains a significant challenge in data assimilation, necessitating ongoing advancements in methodological approaches.

We validate the final temperature estimates using the earliest instrumental data from the Global Historical Climatology Network (GHCN). The results demonstrate the effectiveness of our Celsius-scaled kriged data and Bayesian data assimilation method in improving temperature predictions.

In summary, our data assimilation approach is designed to enhance temperature predictions by integrating REACHES and LME datasets through data transformation, nonstationary time series modeling, and applying Kalman filtering and smoothing. This method provides refined estimates of true temperature states, effectively accounting for uncertainties and capturing heterogeneous temporal variations.

The subsequent sections of this article are structured as follows. Section 2 introduces the datasets employed in this study. Section 3 discusses the application of the best linear predictor on the REACHES data and transforms these data to the Celsius scale. Section 4 presents our Bayesian data assimilation approach, and Section 5 validates the predicted temperatures. Finally, Section 6 offers further discussion.

## **2. Data**

This study utilizes two primary datasets: the REACHES database derived from historical Chinese documents and the LME data based on numerical climate simulations.

### *2.1. REACHES*

The REACHES database compiles climate data from Chinese historical documents spanning the Ming and Qing dynasties. It encompasses various climate variables such as precipitation, temperature, thunder, and crop conditions. The database is accessible at [https:](https://)

Year	Chinese Text	English Translation	Temperature Index
1839	亢陽，地熱如爐	Scorching sun, ground hot as a furnace	1
1428	秋霜	Autumn frost	-1
1644	冬凍，鑿之不入	Winter freeze, impenetrable by chisels	-2

Table 1: Examples of historical text translations into ordinal-scale temperature indices in the REACHES dataset.

[//www.ncdc.noaa.gov/paleo/study/23410](http://www.ncdc.noaa.gov/paleo/study/23410). This study focuses on the temperature data, which are organized chronologically (by year) and geographically (by longitude and latitude). Historical climate databases like REACHES employ ordinal-scale indices to quantitatively represent qualitative descriptions from historical documents. These indices are crucial for translating qualitative historical records into quantifiable data for statistical analysis.

The temperature data in the REACHES dataset are categorized using a four-level ordinal scale that ranges from -2 to 1. This scale is designed to reflect the qualitative assessments in the historical documents, where -2 indicates “very cold”, -1 “cold”, 0 “normal”, and 1 “warm”. This asymmetric scale arises because warm-related records are less frequently documented in Chinese historical texts than cold events, reflecting a cultural emphasis on the more impactful cold weather events in agricultural societies. Table 1 provides examples of how Chinese texts have been converted into these ordinal-scale indices.

Figure 1(a) displays the time series of annual counts of temperature records in the REACHES dataset, showing a marked increase in data volume in more recent periods compared to earlier years. Historical records tend to emphasize unusual weather events, leading to a skewed distribution of temperature levels, as illustrated in Figure 1(b). This pattern confirms that historical documentation prioritizes significant anomalies over typical weather conditions, visually supported by the distribution of temperature indices shown in the figure.

When multiple records from the same location and year are encountered, their temperature indices are averaged to provide a single representative value for that year and location. Figure 2 illustrates the geographical distribution of temperature records across East Asia from the REACHES dataset, spanning from 1368 to 1911. Each point on the map is color-

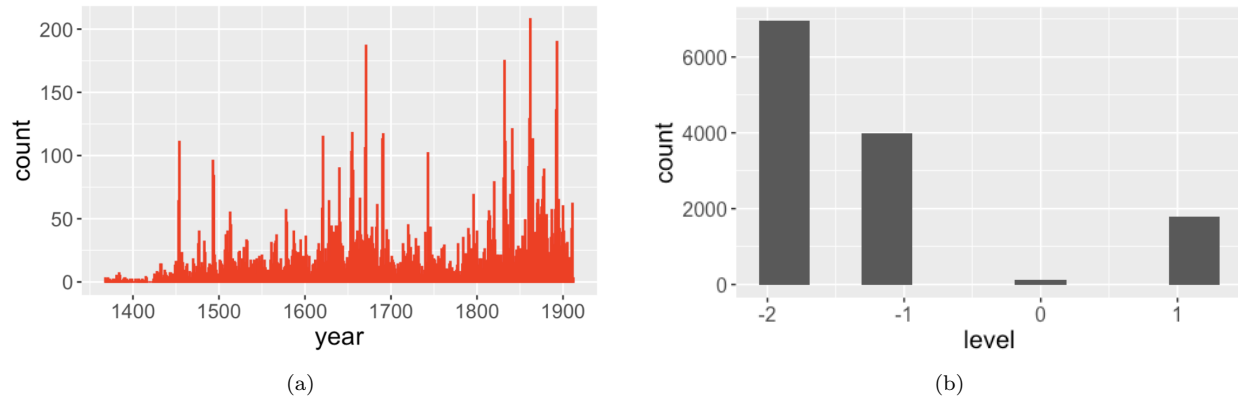


Figure 1: (a) Annual counts of temperature records in the REACHES dataset from 1368 to 1911; (b) Frequency of each temperature category in the REACHES dataset.

coded according to the average temperature index at that location, effectively highlighting the spatial density and distribution of records.

## 2.2. Last Millennium Ensemble

The LME offers a comprehensive global temperature dataset that extends back to 850 CE. This dataset is indexed by time (year) and geolocation (longitude and latitude), achieving a spatial resolution of approximately 2 degrees in both the atmosphere and land components. It incorporates numerical simulations that include natural forcings such as solar irradiance, greenhouse gas concentrations, aerosols, volcanic emissions, orbital parameters, and land-use changes. By integrating all six of these forcings, the LME aims to recreate the dynamics of Earth’s climate over the past millennium (Otto-Bliesner et al., 2016).

Although the LME relies on sophisticated climate model simulations rather than direct instrumental measurements, potentially raising concerns about the precision of specific annual records, its primary strength lies in its ability to provide reliable estimates over extended periods. The dataset’s accuracy is particularly robust over extended timescales, such as decades and centuries, making it highly valuable for historical climate analysis. This characteristic is critical because, while short-term annual variations may be less precise due to modeling uncertainties, the long-term distributions provide reliable insights into climate trends and patterns.

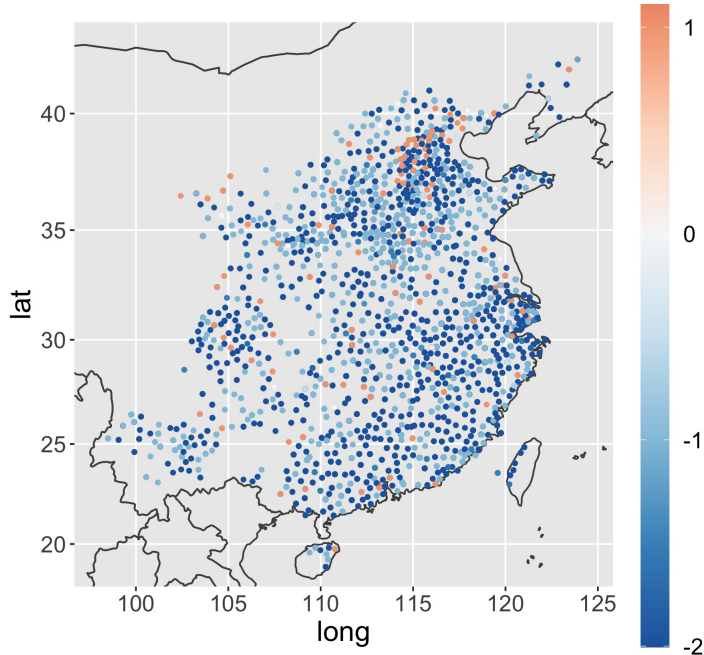


Figure 2: Geographical distribution of temperature records from 1368 to 1911 across East Asia, as documented in the REACHES dataset. Each point is color-coded by the average temperature index, showcasing the spatial distribution and density of recorded temperatures.

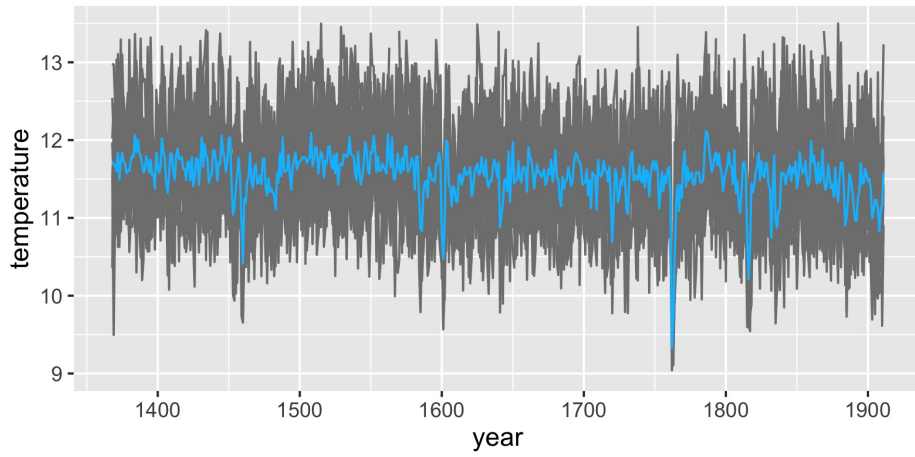
In our research, we utilize the LME as a foundational element to estimate the distribution of historical temperatures, which serves as the prior in our Bayesian data assimilation framework. We specifically employ 13 distinct simulation outputs from the LME, each incorporating all transient forcings, to capture the complete spectrum of climate variability induced by natural factors over the last millennium. Figure 3 shows the 13 LME time series and their averages in Beijing, Shanghai, and Hong Kong. The data can be accessible at <https://www.cesm.ucar.edu/community-projects/lme>.

### 3. Historical Temperature Reconstruction based on REACHES Data

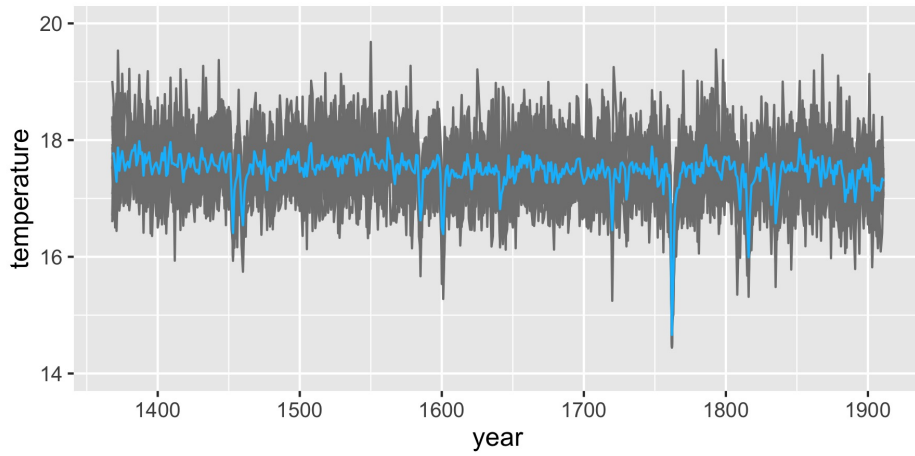
#### 3.1. Kriging with Zero-Mean Spatial Processes based on Interval-Censored Data

The REACHES dataset, derived from historical documents, contains numerous gaps in data for certain years or locations, primarily due to its emphasis on exceptional climatic events. This characteristic likely introduces biases into the dataset, emphasizing extremes over typical weather patterns.

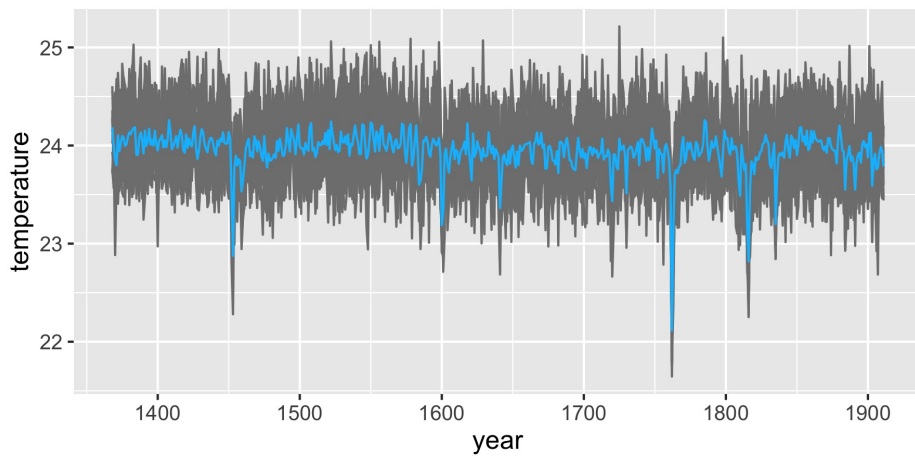
To effectively model these data, we employ a zero-mean spatial Gaussian process  $\{Y_t(\mathbf{s}) :$



(a) Beijing



(b) Shanghai



(c) Hong Kong

Figure 3: Yearly temperature time series data from 13 LME simulations, where the blue curve is the time series averaged over 13 simulations: (a) Beijing; (b) Shanghai; (c) Hong Kong.

$\mathbf{s} \in D\}$ , representing the underlying temperature for the year  $t$  over a geographical region  $D \subset \mathbb{R}^2$ . Opting for a zero-mean model reflects the assumption that normal weather conditions, which are more frequent but less often documented, constitute the baseline state. Given the annual nature of the data, we consider the temporal dependence among  $Y_t(\cdot)$  for years 1368 to 1911 to be minimal and hence treat these processes as independent. Therefore, for notational simplicity, we drop the subscript  $t$  and consider the zero-mean Gaussian spatial process  $\{Y(\mathbf{s}) : \mathbf{s} \in D\}$ . We assume that the process  $Y(\cdot)$  is stationary and has the following exponential covariance function:

$$C_Y(\mathbf{s}, \mathbf{s}^*) \equiv \text{cov}(Y(\mathbf{s}), Y(\mathbf{s}^*)) = \sigma_Y^2 \exp\left(-\frac{\|\mathbf{s} - \mathbf{s}^*\|}{\alpha}\right); \quad \mathbf{s}, \mathbf{s}^* \in D, \quad (1)$$

where  $\sigma_Y^2 = \text{var}(Y(\mathbf{s}))$  and  $\alpha$  is a scale parameter.

The REACHES temperature data, denoted by  $\mathbf{Z} \equiv (Z(\mathbf{s}_1), \dots, Z(\mathbf{s}_n))^T$ , are collected at locations  $\mathbf{s}_1, \dots, \mathbf{s}_n \in D$ . We assume that they are observed by rounding the latent variables:

$$Z^*(\mathbf{s}_i) \equiv Y(\mathbf{s}_i) + \epsilon(\mathbf{s}_i); \quad i = 1, \dots, n,$$

to the nearest integer values in  $\{-2, -1, 0, 1\}$ :

$$Z(\mathbf{s}_i) = h(Z^*(\mathbf{s}_i)); \quad i = 1, \dots, n, \quad (2)$$

where  $\epsilon(\mathbf{s}_i) \sim N(0, \sigma_\epsilon^2)$ ;  $i = 1, \dots, n$ , are white noise, representing measurement errors, and

$$h(x) = \begin{cases} -2; & \text{if } x < -3/2, \\ -1; & \text{if } x \in [-3/2, -1/2), \\ 0; & \text{if } x \in [-1/2, 1/2], \\ 1; & \text{if } x > 1/2, \end{cases}$$

is the rounding function.

Given any location  $\mathbf{s}_0 \in D$ , we apply the best linear predictor to estimate  $Y(\mathbf{s}_0)$ :

$$\hat{Y}(\mathbf{s}_0) = \mathbf{c}_{YZ}(\mathbf{s}_0) \Sigma_Z^{-1} (\mathbf{Z} - \mu_Z \mathbf{1}), \quad (3)$$

where  $\mu_Z = E(Z(\mathbf{s}_i))$ ,  $\mathbf{1}$  is a vector of ones,  $\mathbf{c}_{YZ}(\mathbf{s}_0) \equiv (\text{cov}(Y(\mathbf{s}_0), Z(\mathbf{s}_1)), \dots, \text{cov}(Y(\mathbf{s}_0), Z(\mathbf{s}_n)))^T$ , and  $\Sigma_Z$  is an  $n \times n$  matrix with the  $(i, j)$ -th element  $\text{cov}(Z(\mathbf{s}_i), Z(\mathbf{s}_j))$ , for  $i, j = 1, \dots, n$

(see Cressie, 1993). The corresponding mean-squared prediction error (MSPE) is given by

$$\mathbb{E}(\hat{Y}(\mathbf{s}_0) - Y(\mathbf{s}_0))^2 = C_Y(\mathbf{s}_0, \mathbf{s}_0) - \mathbf{c}_{YZ}(\mathbf{s}_0)^T \boldsymbol{\Sigma}_Z^{-1} \mathbf{c}_{YZ}(\mathbf{s}_0). \quad (4)$$

Due to the rounding of the latent variables  $Z^*(\mathbf{s}_i)$  into discrete indices, the terms  $\mu_Z$ ,  $\boldsymbol{\Sigma}_Z$ , and  $\mathbf{c}_{YZ}$  in (3) and (4) become complex functions of the model parameters  $\alpha$ ,  $\sigma_Y^2$ , and  $\sigma_\varepsilon^2$ . To obtain  $\mu_Z(\alpha, \sigma_Y^2, \sigma_\varepsilon^2)$ , we recognize that  $Z^*(\mathbf{s}_i) \sim N(0, \sigma_Y^2 + \sigma_\varepsilon^2)$ . The cumulative distribution function (CDF) of  $Z^*(\mathbf{s}_i)$  is then given by

$$F^*(x) \equiv P(Z^*(\mathbf{s}_i) \leq x) = \Phi(x / (\sigma_Y^2 + \sigma_\varepsilon^2)^{1/2}),$$

where  $\Phi(\cdot)$  denotes the standard normal CDF. Thus

$$\begin{aligned} \mu_Z &= -2F^*(-3/2) - (F^*(-1/2) - F^*(-3/2)) + (1 - F^*(1/2)) \\ &= -F^*(-3/2) = -\Phi(-3 / \{2(\sigma_Y^2 + \sigma_\varepsilon^2)^{1/2}\}). \end{aligned}$$

The covariance terms  $\mathbf{c}_{YZ}(\alpha, \sigma_Y^2, \sigma_\varepsilon^2)$  and  $\boldsymbol{\Sigma}_Z(\alpha, \sigma_Y^2, \sigma_\varepsilon^2)$  in equations (3) and (4) have no closed-form expressions due to the interval censoring. However, they can be evaluated numerically using the properties of interval-censored normal distributions. Specifically, each element  $\text{cov}(Y(\mathbf{s}_0), Z(\mathbf{s}_i))$  involves computing the covariance between a continuous normal variable  $Y(\mathbf{s}_0)$  and an interval-censored variable  $Z(\mathbf{s}_i)$ . This requires integrating the bivariate normal distribution over the intervals defined by  $Z(\mathbf{s}_i)$ . For  $\boldsymbol{\Sigma}_Z$ , each element  $\text{cov}(Z(\mathbf{s}_i), Z(\mathbf{s}_j))$  involves computing the covariance between two interval-censored normal variables. This necessitates evaluating the probabilities and expectations over the two-dimensional regions defined by the observed indices. These numerical evaluations are standard in the analysis of interval-censored data and can be efficiently computed using existing statistical software packages that implement algorithms for multivariate normal probabilities and expectations (Genz and Bretz, 2009).

By treating the rounding of  $Z^*(\mathbf{s}_i)$  as interval censoring, we appropriately account for the uncertainty introduced by discretization. This approach allows us to accurately estimate

$\mu_Z$ ,  $\mathbf{c}_{YZ}$ , and  $\Sigma_Z$ , enabling the application of kriging methods to the REACHES dataset despite the lack of closed-form expressions.

Due to interval censoring, we estimate the model parameters  $\alpha$ ,  $\sigma_Y^2$ , and  $\sigma_\varepsilon^2$  in (1) and (2) using a two-step procedure. In the first step, we compute the empirical variograms by pooling all the data from all years and fit the exponential variogram model with a nugget effect using weighted least squares (Cressie, 1985). This provides initial estimates  $\tilde{\alpha}$ ,  $\tilde{\sigma}_Y^2$ , and  $\tilde{\sigma}_\varepsilon^2$ , obtained without considering interval censoring.

In the second step, we account for interval censoring by deriving bias-corrected functions:

$$f_1(\sigma_Y^2 + \sigma_\varepsilon^2) \equiv \text{var}(Z(\mathbf{s})), \quad (5)$$

$$f_2(\sigma_\varepsilon^2) \equiv \lim_{\|\mathbf{s}-\mathbf{s}'\| \rightarrow 0} \text{var}(Z(\mathbf{s}) - Z(\mathbf{s}'))/2, \quad (6)$$

$$f_3(\alpha) \equiv \arg \min_{\alpha > 0} \int_0^\infty \{C_Z(x; \alpha) - \sigma_Y^2 \exp(-x/\alpha)\}^2 dx, \quad (7)$$

where

$$C_Z(x; \alpha) \equiv \text{cov}(h(Z^*(\mathbf{s})), h(Z^*(\mathbf{s}'))), \quad \alpha > 0, x = \|\mathbf{s} - \mathbf{s}'\| > 0.$$

Since the right-hand sides of  $f_1(\cdot)$ ,  $f_2(\cdot)$ , and  $f_3(\cdot)$  in (5)–(7) can be estimated by  $\tilde{\sigma}_Y^2 + \tilde{\sigma}_\varepsilon^2$ ,  $\tilde{\sigma}_\varepsilon^2$ , and  $\tilde{\alpha}$ , respectively, we obtain our final estimates of  $\alpha$ ,  $\sigma_Y^2$ , and  $\sigma_\varepsilon^2$  as follows:

$$\hat{\alpha} = f_3^{-1}(\tilde{\alpha}), \quad \hat{\sigma}_Y^2 = f_1^{-1}(\tilde{\sigma}_Y^2 + \tilde{\sigma}_\varepsilon^2) - f_2^{-1}(\tilde{\sigma}_\varepsilon^2), \quad \hat{\sigma}_\varepsilon^2 = f_2^{-1}(\tilde{\sigma}_\varepsilon^2).$$

We proceed to derive  $f_1(\cdot)$ ,  $f_2(\cdot)$ , and  $f_3(\cdot)$ , with details provided below.

- Derivation of  $f_1(\sigma_Y^2 + \sigma_\varepsilon^2)$ : For given values of  $\sigma_Y^2$  and  $\sigma_\varepsilon^2$ , we use a Monte Carlo (MC) method by generating an independent and identically distributed (i.i.d.) MC sample  $\{Z(\mathbf{s})\}$ . This allows us to estimate  $\text{var}(Z(\mathbf{s}))$  under interval censoring.
- Derivation of  $f_2(\sigma_\varepsilon^2)$ : With a given value of  $\sigma_\varepsilon^2$ , we compute  $\text{var}(h(Y + \epsilon_1) - h(Y + \epsilon_2))/2$  using an MC sample where  $Y \sim N(0, f_1^{-1}(\tilde{\sigma}_Y^2 + \tilde{\sigma}_\varepsilon^2) - \sigma_\varepsilon^2)$  and  $(\epsilon_1, \epsilon_2)' \sim N(\mathbf{0}, \sigma_\varepsilon^2 \mathbf{I})$  independently. This step accounts for the measurement error variance in the nugget effect.

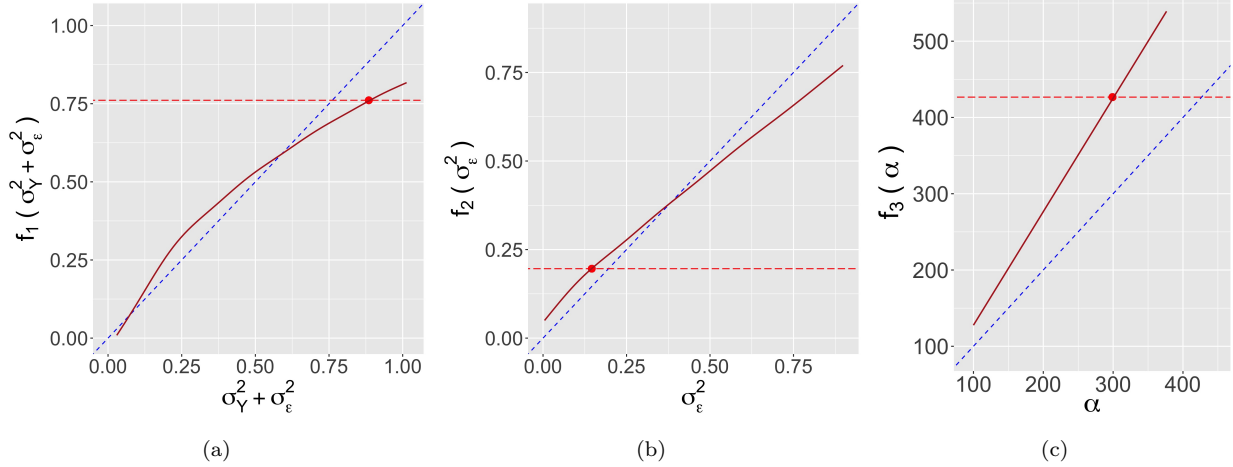


Figure 4: Calibration functions for model parameters: (a)  $f_1(\cdot)$  for  $\sigma_Y^2 + \sigma_\epsilon^2$ , (b)  $f_2(\cdot)$  for  $\sigma_\epsilon^2$ , and (c)  $f_3(\cdot)$  for  $\alpha$ , each represented by a red solid line. The red horizontal dashed line indicates the initial estimates for each parameter. The blue dashed lines, showing 45-degree lines, serve as a reference for identifying deviations from a one-to-one correspondence between the estimated and true values.

- Derivation of  $f_3(\alpha)$ : For a given value of  $\alpha$ , we generate an MC sample  $\{Z^*(\mathbf{s})\}$  using  $\sigma_Y^2$  and  $\sigma_\epsilon^2$  provided by  $\hat{\sigma}_Y^2$  and  $\hat{\sigma}_\epsilon^2$ , respectively. We then compute  $C_Z(x; \alpha)$  and minimize the integral in (7) to solve for  $\alpha$ , correcting for the bias introduced by interval censoring in spatial correlation estimation.

Figure 4(a)-(c) shows the calibration functions,  $f_1(\cdot)$ ,  $f_2(\cdot)$ , and  $f_3(\cdot)$ , respectively. The initial estimates of the parameters  $(\alpha, \sigma_Y^2, \sigma_\epsilon^2)'$  are given by  $(\tilde{\alpha}, \tilde{\sigma}_Y^2, \tilde{\sigma}_\epsilon^2)' = (426.7, 0.564, 0.197)$ , and the final estimates, after applying bias correction, are  $(\hat{\alpha}, \hat{\sigma}_Y^2, \hat{\sigma}_\epsilon^2)' = (299.1, 0.739, 0.146)$ . Figures 5 and 6 display the original REACHES temperature data alongside the surfaces predicted using the best linear predictor (after substituting the final parameter estimates  $(\hat{\alpha}, \hat{\sigma}_Y^2, \hat{\sigma}_\epsilon^2)'$ ) for the years 1465 and 1851, respectively. Figure 7(a) presents the annual temperature time series for Beijing, derived from the best linear predictions.

### 3.2. Quantile Mapping to Convert Kriged REACHES Data to Celsius Scale

Although the kriged REACHES surfaces provide historical temperature estimates at any location from 1368 to 1911, these estimates are not expressed on the Celsius scale. To convert the kriged REACHES data into Celsius temperatures, we utilize information from the LME data for the same period by applying quantile mapping.

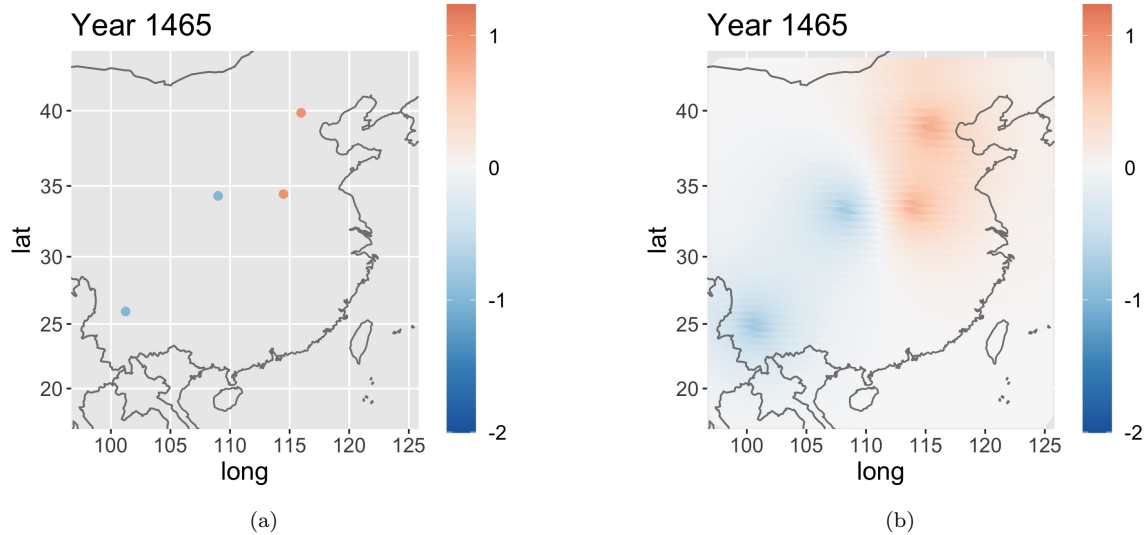


Figure 5: (a) The REACHES temperature data for the year 1465; (b) The predicted surface obtained from the best linear predictor based on the data in (a).

Let  $\hat{Y}_1, \dots, \hat{Y}_N$  represent the kriged REACHES temperature data at a specific location from 1368 to 1911, which we assume are identically distributed with a continuous cumulative distribution function (CDF)  $F_{\hat{Y}}$ . Similarly, let  $x_1, \dots, x_N$  denote the corresponding averaged LME temperature data over the 13 simulation outputs at the same location, assumed to be identically distributed with a continuous CDF  $F_x$ . Since  $F_{\hat{Y}}(\hat{Y}_t)$  and  $F_x(x_t)$  are uniformly distributed on  $(0, 1)$  for  $t = 1, \dots, N$ , we can establish the following relationship:

$$F_x^{-1}(F_{\hat{Y}}(\hat{Y}_t)) \sim F_x, \quad t = 1, \dots, N. \quad (8)$$

This mapping effectively transforms the REACHES data  $\hat{Y}_t$  into the Celsius scale by matching the quantiles of the REACHES data distribution to those of the LME data distribution.

Based on exploratory data analysis, we assume that the REACHES temperature data  $\{\hat{Y}_t\}$  follow a normal distribution, whereas the LME temperature data  $\{x_t\}$  follow a skew-normal distribution. We apply maximum likelihood estimation to determine the parameters of these distributions, obtaining the estimated CDFs  $\hat{F}_{\hat{Y}}$  and  $\hat{F}_x$ . This leads to the calibration function  $g(\cdot)$ , which is described as follows:

$$g(y) = \hat{F}_x^{-1}(\hat{F}_{\hat{Y}}(y)). \quad (9)$$

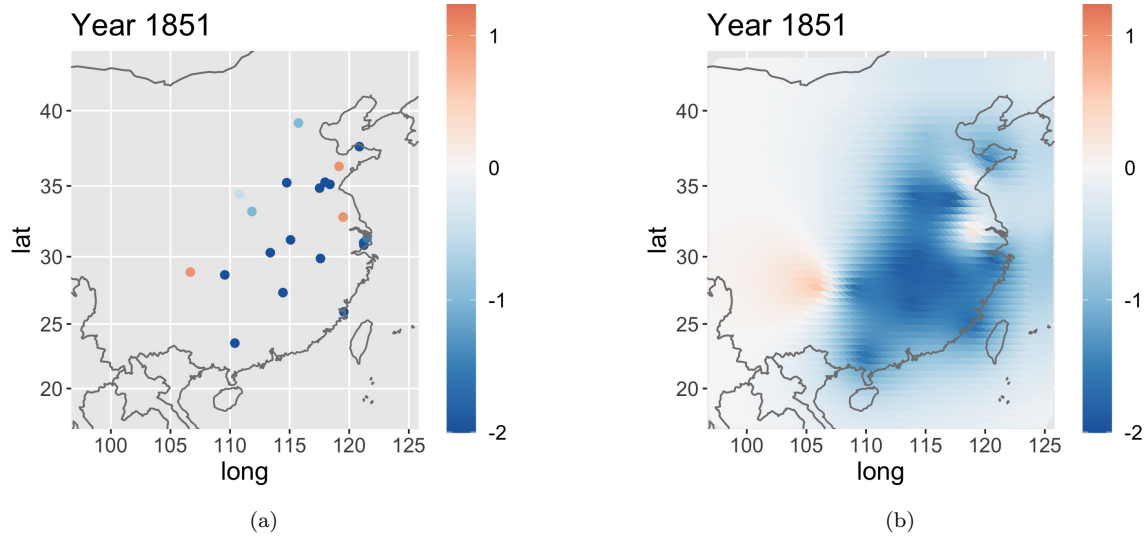


Figure 6: (a) The REACHES temperature data for the year 1851; (b) The predicted surface obtained from the best linear predictor based on the data in (a).

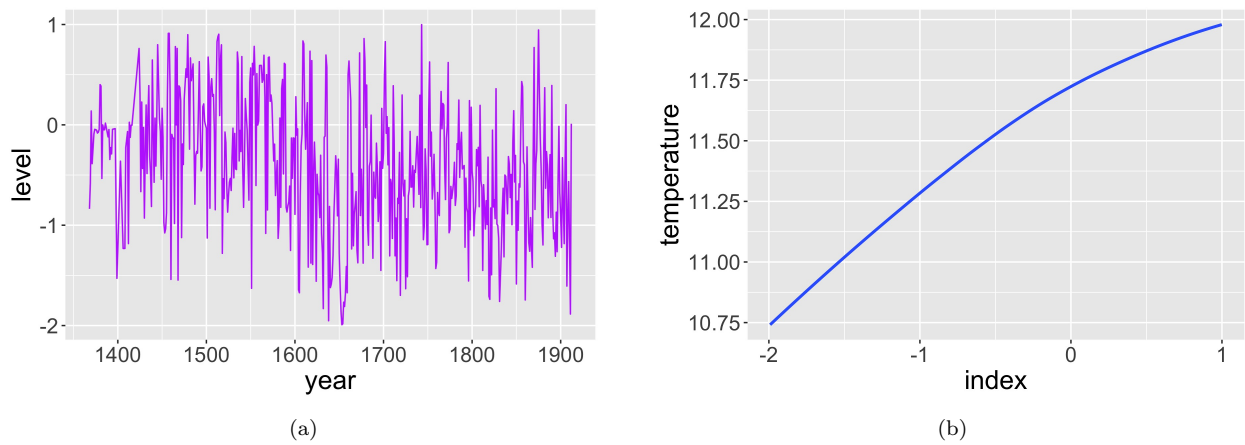


Figure 7: (a) Annual temperature time series for Beijing based on kriged REACHES data; (b) Estimated calibration function transforming REACHES temperature indices in Beijing to the Celsius scale.

The estimated probability density functions (PDFs) are depicted in Figure 8. The resulting calibration function that converts the REACHES indices to the Celsius scale is shown in Figure 7 (b).

Recall that the MSPE for the kriging predictor  $\hat{Y}_t$  of  $Y_t$  is given by equation (4). Applying a Taylor expansion to  $g(\hat{Y}_t)$  around  $Y_t$ , the MSPE of  $g(\hat{Y}_t)$  is approximately:

$$\mathbb{E}[g(\hat{Y}_t) - g(Y_t)]^2 \approx [g'(\hat{Y}_t)]^2 \mathbb{E}(\hat{Y}_t - Y_t)^2 = \left( \frac{\hat{f}_{\hat{Y}}(\hat{Y}_t)}{\hat{f}_x(g(\hat{Y}_t))} \right)^2 \mathbb{E}(\hat{Y}_t - Y_t)^2, \quad (10)$$

where  $\hat{f}_{\hat{Y}}(y) \equiv \hat{F}'_{\hat{Y}}(y)$  and  $\hat{f}_x(y) \equiv \hat{F}'_x(y)$  are the estimated PDFs of  $\hat{Y}_t$  and  $x_t$ , respectively.

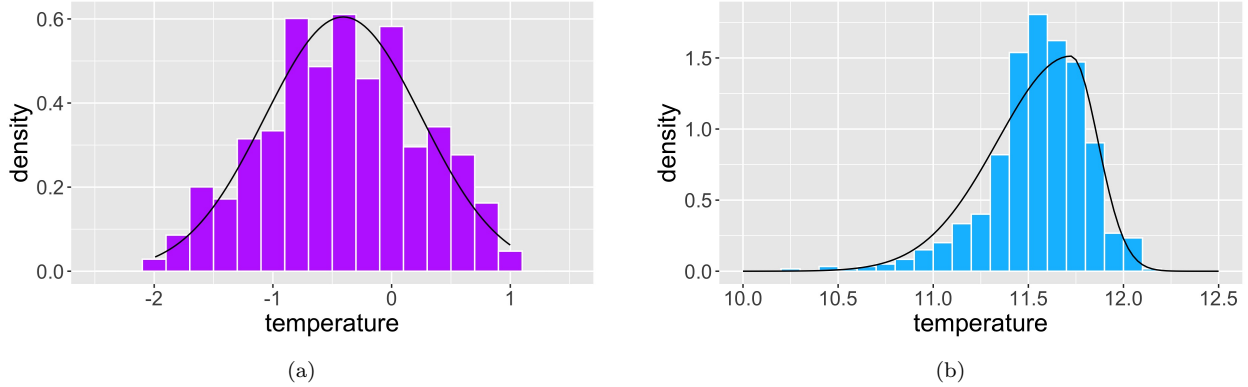


Figure 8: Histogram of Beijing temperature data and the corresponding PDF estimate: (a) REACHES data with estimated normal PDF; (b) LME data with estimated skew normal PDF.

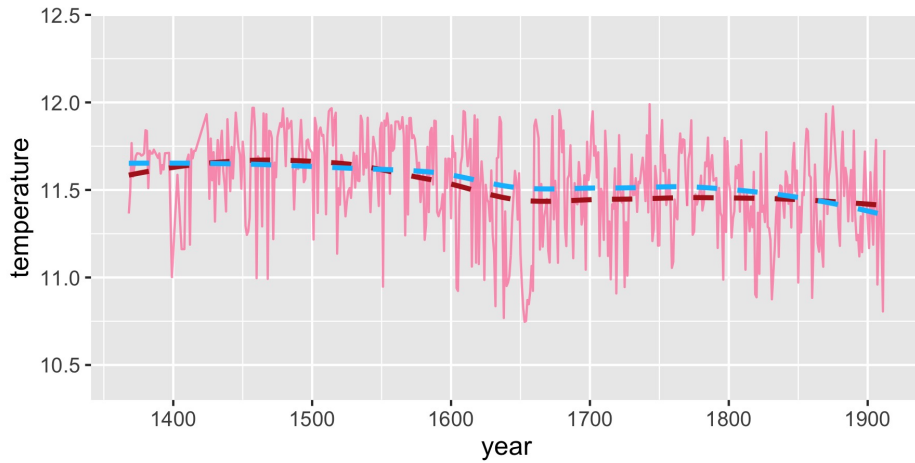
This leads to a noisy time series,  $X_t^* \equiv g(\hat{Y}_t)$ ;  $t = 1, \dots, N$ , which can be approximately given by

$$X_t^* = X_t + \delta_t; \quad t = 1, \dots, N. \quad (11)$$

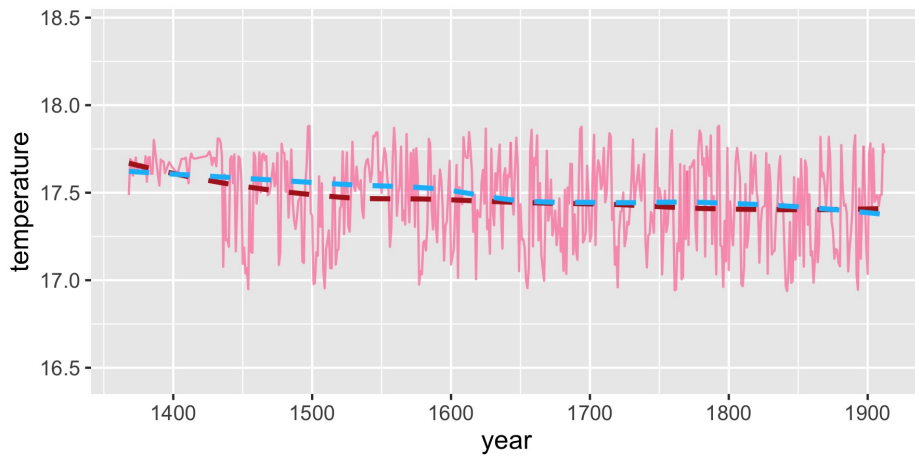
where  $X_t \equiv g(Y_t)$  is the true Celsius-scale temperature and  $\delta_t \sim N(0, v_t^2)$  is the corresponding error, independent of  $X_t$ ;  $t = 1, \dots, N$ .

The Celsius-scale REACHES data  $\{X_t^*\}$  given by (11) for Beijing, Shanghai, and Hong Kong, transformed through function  $g(\cdot)$ , are depicted in Figure 9. The LOESS (Locally Estimated Scatterplot Smoothing) fits, shown as blue and red dashed curves for the LME and the Celsius-scale REACHES data, respectively, apply a local regression model to the data, capturing long-term patterns for the two sources (Cleveland, 1979). Despite the inherent limitations in the two datasets, these LOESS curves suggest an underlying consistency between the datasets, highlighting their complementary nature and providing a smoothed interpretation of the data trends.

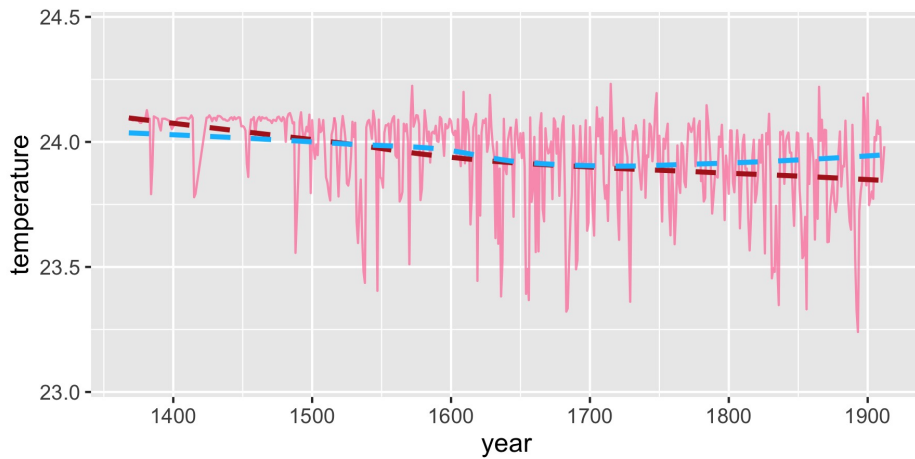
The Celsius-scale REACHES data and the LME outputs, despite their fundamentally different origins, exhibit similar long-term patterns, indicating that they capture consistent historical climate signals. The REACHES dataset, derived from qualitative historical documents that record extreme weather events and anomalies, and the LME data, generated from climate model simulations integrating various natural forcings, both reflect significant climatic phenomena. This alignment lends credibility to both datasets as reliable represen-



(a)



(b)



(c)

Figure 9: Time series plots of Celsius-scaled REACHES data from 1368 to 1911. The red and blue dashed curves represent the LOESS fits of the REACHES data and the LME data, respectively: (a) Beijing; (b) Shanghai; (c) Hong Kong.

tations of historical climate variations in East Asia.

Notably, major climatic events such as the Little Ice Age, a period from approximately the 14th to the 19th century characterized by cooler temperatures worldwide, especially in Europe, North America, and Asia, are consistently captured in both observational proxies and model simulations (Jones and Mann, 2004; Zheng et al., 2014; Fan, 2023). The ability of the REACHES data to reflect long-term climate patterns underscores the value of historical documents as effective proxies for climate reconstruction. This consistency demonstrates that despite the sparsity and potential biases of historical records, they can offer significant insights into historical climate trends when properly processed and calibrated.

#### **4. Bayesian Data Assimilation**

Since the REACHES dataset is constructed from historical documents, its accuracy is highly uncertain. To enhance the precision of our climate reconstruction, we employ a Bayesian data assimilation framework that integrates both the REACHES data and the LME temperature simulations. This framework has been widely applied across various scientific disciplines to combine observational data with model-based predictions, effectively accounting for uncertainties in both sources (Wikle and Berliner, 2007). In this study, we focus on Beijing, Shanghai, and Hong Kong to illustrate our analysis, as these cities have the largest number of temperature records prior to 1912.

We propose a nonstationary first-order autoregressive model (see, e.g., Tsay 2005) to form the prior temperature, using the LME data to estimate the model parameters and treating the resulting distribution as the prior. We then integrate the Celsius-scale REACHES data to estimate the posterior distribution using the Kalman filter and smoother algorithms.

#### 4.1. Prior Derivation

We assume that the state process follows a known transition model  $p(X_t|X_{t-1})$ , which can be expressed as:

$$X_t - \mu_t = M_{t-1}(X_{t-1} - \mu_{t-1}) + \eta_t, \quad \eta_t \sim N(0, r_t^2); \quad t = 2, \dots, N, \quad (12)$$

$$X_1 \sim N(\mu_1, r_1^2), \quad (13)$$

where  $X_t$  denotes the true temperature (state variable) at time  $t$ ,  $\mu_t = \mathbb{E}(X_t)$  is the expected value of  $X_t$ ,  $M_{t-1}$  is an AR parameter describing the temporal evolution of the process, and  $\eta_t$  represents the process noise, which is assumed to be independent of  $X_{t-1}$ , for  $t = 1, \dots, N$ .

The prior model defined by (12) and (13) encapsulates our knowledge about the temporal evolution of the temperature state based on the LME simulations. By estimating the parameters from the LME data, we construct a prior distribution that reflects both the physical dynamics captured by the climate model and the variability inherent in the simulations.

Let  $\boldsymbol{\theta} = (\mu_1, \dots, \mu_n, r_1^2, \dots, r_n^2, M_1, \dots, M_{n-1})'$  denote the collection of parameters in the model given by (12) and (13). To estimate  $\boldsymbol{\theta}$ , we employ the LME data using regularized maximum likelihood with a fused lasso penalty, encouraging both sparsity and smoothness in the parameter estimates.

The LME dataset consists of 13 temperature time series simulations. We denote the temperature at time  $t$  in the  $j$ -th simulation as  $X_t^{(j)}$ , for  $j = 1, \dots, 13$ . We define  $\mathbf{X}^{(j)} = (X_1^{(j)}, \dots, X_n^{(j)})'$  as the  $j$ -th time series and organize all LME simulations into a matrix  $\mathbf{X} = (\mathbf{X}^{(1)}, \dots, \mathbf{X}^{(13)})$ . Under (12) and (13), the negative log-likelihood function for the  $j$ -th time series is given by:

$$h(\mathbf{X}^{(j)}; \boldsymbol{\theta}) = \frac{1}{2} \sum_{t=1}^T \log(r_t^2) + \frac{(x_1^{(j)} - \mu_1)^2}{2r_1^2} + \sum_{t=2}^T \frac{(X_t^{(j)} - \mu_t - M_{t-1}(X_{t-1}^{(j)} - \mu_{t-1}))^2}{2r_t^2} + \text{constant}.$$

Aggregating over all simulations while promoting smoothness among neighboring parameters, we consider the negative log-likelihood with a fused lasso penalty:

$$g(\mathbf{X}; \boldsymbol{\theta}) = \sum_{j=1}^{13} h(\mathbf{X}^{(j)}; \boldsymbol{\theta}) + \lambda_1 \sum_{t=1}^{n-1} |M_t| + \lambda_2 \sum_{t=1}^{n-2} |M_{t+1} - M_t| + \lambda_3 \sum_{t=1}^{n-1} |\mu_{t+1} - \mu_t|, \quad (14)$$

where  $\lambda_1 \geq 0$ ,  $\lambda_2 \geq 0$ , and  $\lambda_3 \geq 0$  are tuning parameters controlling the degree of regularization. The first penalty term encourages sparsity in the  $\{M_t\}$  coefficients, the second promotes smoothness across time for the  $\{M_t\}$ , and the third enforces smoothness in the mean parameters  $\{\mu_t\}$ . Our goal is to estimate the parameter vector  $\boldsymbol{\theta}$  by minimizing the penalized negative log-likelihood function:

$$\hat{\boldsymbol{\theta}}_{\lambda_1, \lambda_2, \lambda_3} = \arg \min_{\boldsymbol{\theta}} g(\mathbf{X}; \boldsymbol{\theta}). \quad (15)$$

Including the fused lasso penalty serves to regularize the parameter estimates, mitigating overfitting and ensuring that the estimated parameters exhibit temporal smoothness, a reasonable assumption for climate variables that change gradually over time. However, due to the absence of closed-form solutions for  $\hat{\boldsymbol{\theta}}_{\lambda_1, \lambda_2, \lambda_3}$ , we employ an iterative algorithm to estimate the parameters. Specifically, we use the R package `penalized` (Goeman, 2022), which implements efficient coordinate descent methods suitable for high-dimensional optimization problems with lasso-type penalties. The detailed steps are given below:

1. Initialization:  $\mu_t = \frac{1}{13} \sum_{j=1}^{13} X_t^{(j)}$  and  $r_t^2 = \frac{1}{13} \sum_{j=1}^{13} (X_t^{(j)} - \mu_t)^2$ , for  $t = 1, \dots, N$ .
2. Estimate  $M_t$ : With  $\mu_t$  and  $r_t^2$  fixed, estimate  $M_t$  by minimizing  $g(\mathbf{X}; \boldsymbol{\theta})$  with respect to  $M_t$ , using the `penalized` package to handle the fused lasso penalty.
3. Update  $\mu_t$ : With  $r_t^2$  and  $M_t$  fixed, estimate  $\mu_t$  by minimizing  $g(\mathbf{X}; \boldsymbol{\theta})$  with respect to  $\mu_t$ , again using the `penalized` package.
4. Update  $r_t^2$ : With  $\mu_t$  and  $M_t$  fixed, update  $r_t^2$  using the closed-form solution:

$$r_1^2 = \frac{1}{13} \sum_{j=1}^{13} \left( X_1^{(j)} - \mu_1 \right)^2,$$

$$r_t^2 = \frac{1}{13} \sum_{j=1}^{13} \left( X_t^{(j)} - \mu_t - M_{t-1} \left( X_{t-1}^{(j)} - \mu_{t-1} \right) \right)^2, \quad \text{for } t = 2, \dots, n.$$

5. Repeat steps 2-4 until convergence criteria are met (e.g., changes in parameter estimates fall below a predefined threshold).

The choice of tuning parameters  $\lambda_1$ ,  $\lambda_2$ , and  $\lambda_3$  is crucial in the estimation process. When  $\lambda_1 = 0$ ,  $\lambda_2 = 0$ , and  $\lambda_3 = 0$ , the method reduces to the standard maximum likelihood

estimation. As  $\lambda_1 \rightarrow \infty$ , the estimates of the coefficients  $M_t$  shrink toward zero, promoting sparsity in the model. Conversely, as  $\lambda_2 \rightarrow \infty$  and  $\lambda_3 \rightarrow \infty$ , the estimates of  $M_t$  and  $\mu_t$  converge to constant values corresponding to a stationary time series, enhancing smoothness over time by reducing variability among adjacent parameters.

To determine the optimal tuning parameters, we perform 13-fold cross-validation, where each fold contains a single LME time series. We treat the  $l$ -th time series as the testing data in each iteration and use the remaining 12 as the training data. Let  $\hat{\boldsymbol{\theta}}_{\lambda_1, \lambda_2, \lambda_3}^{(-l)}$  denote the estimated parameters based on the training data obtained by solving:

$$\hat{\boldsymbol{\theta}}_{\lambda_1, \lambda_2, \lambda_3}^{(-l)} = \arg \min_{\boldsymbol{\theta}} \left\{ \sum_{j \neq l} h(\mathbf{X}^{(j)}; \boldsymbol{\theta}) + \lambda_1 \sum_{t=1}^{n-1} |M_t| + \lambda_2 \sum_{t=1}^{n-2} |M_{t+1} - M_t| + \lambda_3 \sum_{t=1}^{n-1} |\mu_{t+1} - \mu_t| \right\}.$$

We then compute the cross-validation score:

$$CV_{\lambda_1, \lambda_2, \lambda_3} = \frac{1}{13} \sum_{l=1}^{13} h(\mathbf{X}^{(l)}; \hat{\boldsymbol{\theta}}_{\lambda_1, \lambda_2, \lambda_3}^{(-l)}).$$

We select the tuning parameters  $\lambda_i > 0$ , for  $i = 1, 2, 3$ , that minimize  $CV_{\lambda_1, \lambda_2, \lambda_3}$ .

Figure 10 illustrates the estimated  $M_t$  obtained using the fused lasso penalty, alongside the estimates derived from the maximum likelihood solution ( $\lambda_1 = 0$ ,  $\lambda_2 = 0$ ,  $\lambda_3 = 0$ ). Notably, the fused lasso estimates exhibit pronounced smoothness over time and enhanced sparsity, as adjacent  $M_t$  values are more similar, and some coefficients may be shrunk toward constants. Figure 11 shows the estimated  $\mu_t$  employing the fused lasso penalty, along with the average LME temperature (the yearly average of the 13 LME time series). The plot shows smooth transitions observed among adjacent  $\mu_t$  values when employing the fused lasso penalty, indicating that the estimated mean temperatures vary gradually over time, aligning with the expected temperature behavior.

#### 4.2. Posterior Derivation

Our objective is to estimate the posterior distribution of the true temperature state  $X_t$  given all observations up to time  $N$ , that is,  $p(X_t | X_1^*, \dots, X_N^*)$  for  $t = 1, \dots, N$ , where  $X_t^*$  denotes the Celsius-scale REACHES observations as defined in (11). Specifically, we

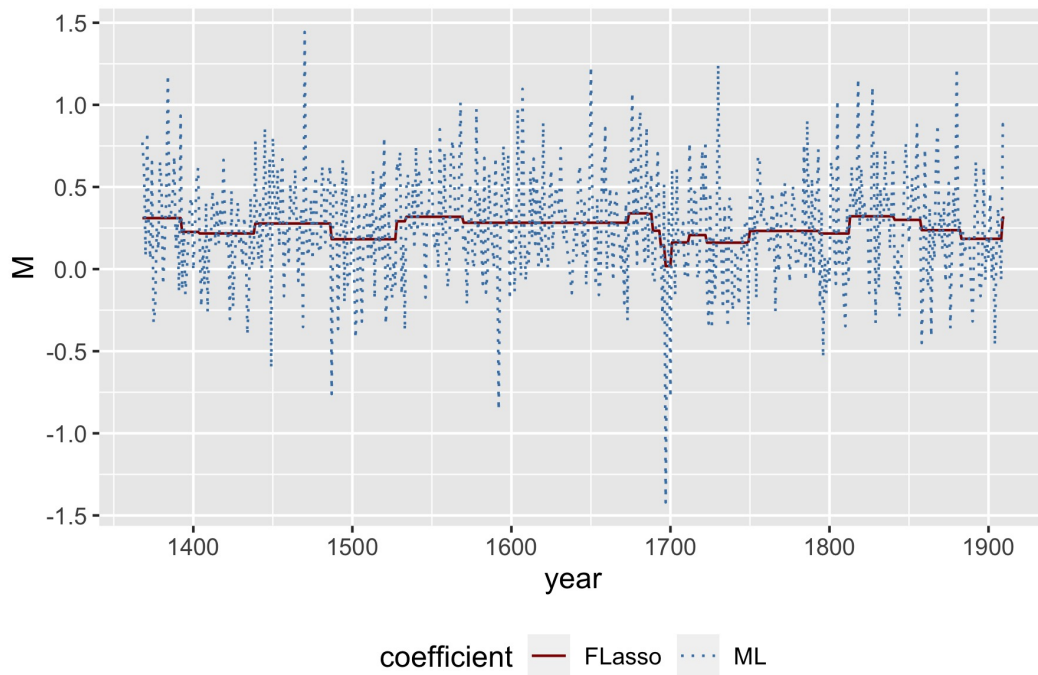


Figure 10: Time series plot of the estimated parameter  $M_t$  from years 1368 to 1911. The fused lasso estimates (FLasso) are in dark red, while the maximum likelihood estimates (ML) are in steel blue.

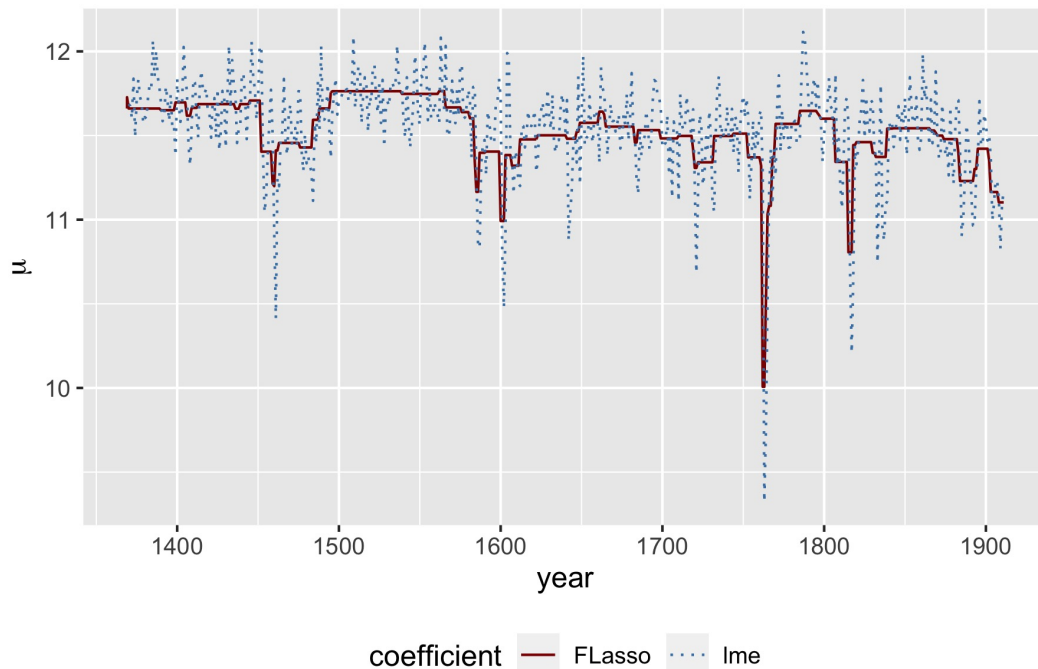


Figure 11: Time series plot of the estimated parameter  $\mu_t$  and the LME temperature (the average of the 13 LME time series by year) from years 1368 to 1911. The fused lasso estimates (FLasso) of  $\mu_t$  are shown in red, and the LME temperature is in a deep sky blue.

aim to compute the posterior mean  $X_{t|N} \equiv \mathbb{E}(X_t|X_1^*, \dots, X_N^*)$  and the posterior variance  $P_{t|n} \equiv \text{var}(X_t|X_1^*, \dots, X_N^*)$  based on the nonstationary time series model described in (12) and (13).

To achieve this, we employ the Kalman filter and smoother algorithms within a Bayesian data assimilation framework. Our method belongs to the offline (or batch) data assimilation techniques, as we collectively process the entire dataset rather than assimilating data sequentially in real time.

The Kalman filter provides an efficient recursive solution for estimating the state of a linear dynamic system from a series of noisy measurements. It operates in two steps: the prediction step and the update step. In the prediction step, we use the prior model to project the state estimate forward in time, calculating the prior estimates  $X_{t|t-1}$  and their uncertainties  $P_{t|t-1}$ :

$$X_{t|t-1} = \mu_t + M_{t-1}(X_{t-1|t-1} - \mu_{t-1}), \quad (16)$$

$$P_{t|t-1} = M_{t-1}^2 P_{t-1|t-1} + r_t^2, \quad (17)$$

where  $X_{t|t-1}$  is the prior estimate of  $X_t$  given observations up to time  $t-1$ , and  $P_{t|t-1}$  is the associated prior variance, for  $t = 2, \dots, N$ .

In the update step, we incorporate the new observation  $X_t^*$  to obtain the posterior estimates  $X_{t|t}$  and  $P_{t|t}$ :

$$K_t = \frac{P_{t|t-1}}{P_{t|t-1} + v_t^2}, \quad (18)$$

$$X_{t|t} = X_{t|t-1} + K_t(X_t^* - X_{t|t-1}), \quad (19)$$

$$P_{t|t} = (1 - K_t)P_{t|t-1}, \quad (20)$$

where  $K_t$  is the Kalman gain, determining the weighting between the prior estimate and the new observation, for  $t = 2, \dots, N$ .

After processing all observations using the Kalman filter, we apply the Kalman smoother to refine the state estimates by incorporating information from all observations. The Kalman

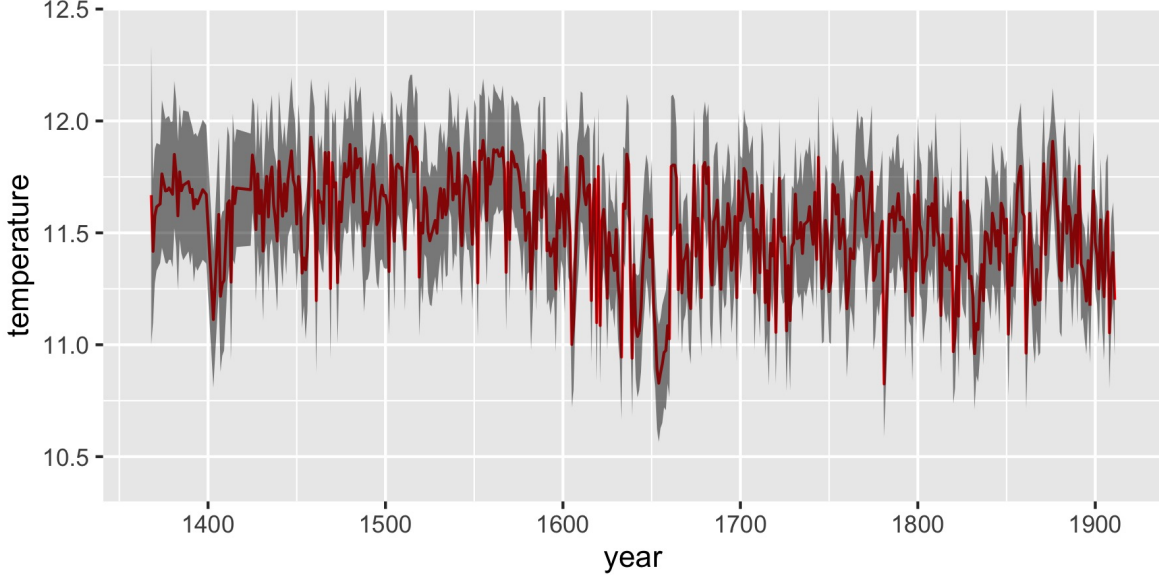


Figure 12: Predicted temperature and its estimated standard deviation from 1368 to 1911 in Beijing.

smoother provides the posterior estimates  $X_{t|n}$  and  $P_{t|n}$  for all  $t = 1, \dots, N$ , using both past and future data:

$$J_t = P_{t|t} M_t P_{t+1|t}^{-1}, \quad (21)$$

$$X_{t|n} = X_{t|t} + J_t (X_{t+1|n} - X_{t+1|t}), \quad (22)$$

$$P_{t|n} = P_{t|t} + J_t (P_{t+1|n} - P_{t+1|t}) J_t', \quad (23)$$

where  $J_t$  is the smoother gain.

By integrating the Kalman filter and smoother, we obtain posterior estimates that are optimal in the least-squares sense for linear Gaussian models, leveraging all available observations. Figure 12 displays the smoothed state estimates  $X_{t|n}$  along with their estimated standard deviations  $P_{t|n}^{1/2}$  for Beijing from 1368 to 1911. Notably, the uncertainty in the estimates has decreased in more recent years due to increased data availability.

This off-line data assimilation method effectively combines the strengths of the LME simulations and the historical observations from REACHES. By systematically updating our state estimates using both prior information and observational data, we achieve a more accurate and reliable reconstruction of historical temperatures.

## 5. Assessment of Predicted Temperature Reliability

Upon obtaining predicted temperature data, assessing their reliability is crucial, particularly within the historical context of the Ming and Qing dynasties. This period presents challenges due to the scarcity of precise instrumental records. Nevertheless, the Global Historical Climatology Network (GHCN) provides instrumental temperature records for China from the mid-19th century, with observations beginning in 1861 in Beijing, 1857 in Shanghai, and 1853 in Hong Kong. Despite potential inaccuracies from early mercury thermometers, these records are invaluable benchmarks for validating our predicted temperatures (Brönnimann et al., 2019). Monthly GHCN data are accessible at <https://www.ncei.noaa.gov/products/land-based-station/global-historical-climatology-network-monthly>.

To evaluate the reliability of our predictions, we convert the monthly GHCN data into annual aggregates and compare these with three methodologies: Celsius-transformed REACHES predictions generated from our kriging and quantile mapping method, LME simulation outputs, and our Bayesian assimilated predictions. Figures 13, 14, and 15 present scatter plots of GHCN data against the three methods in Beijing, Shanghai, and Hong Kong, respectively. Generally, the temperature ranges obtained from the three methods are narrower than those from the GHCN records, reflecting the limitations inherent in historical and model-based data. Except in Beijing, temperatures from all three methods tend to be higher than those from GHCN, possibly due to regional biases or systematic differences in the datasets.

Notably, even though the Celsius-transformed REACHES predictions are derived exclusively from historical documents, we obtain significant correlations with GHCN records. The correlation coefficient reaches an impressive 0.50 in Beijing, indicating the effectiveness of our method in extracting climatic information from historical narratives. This strong correlation suggests that the historical records from Beijing capture climatic variations that closely align with instrumental records. This could be attributed to more precise historical reporting in Beijing, possibly due to its larger daily and seasonal temperature fluctuations or climatic characteristics that render temperature variations in Beijing more indicative of

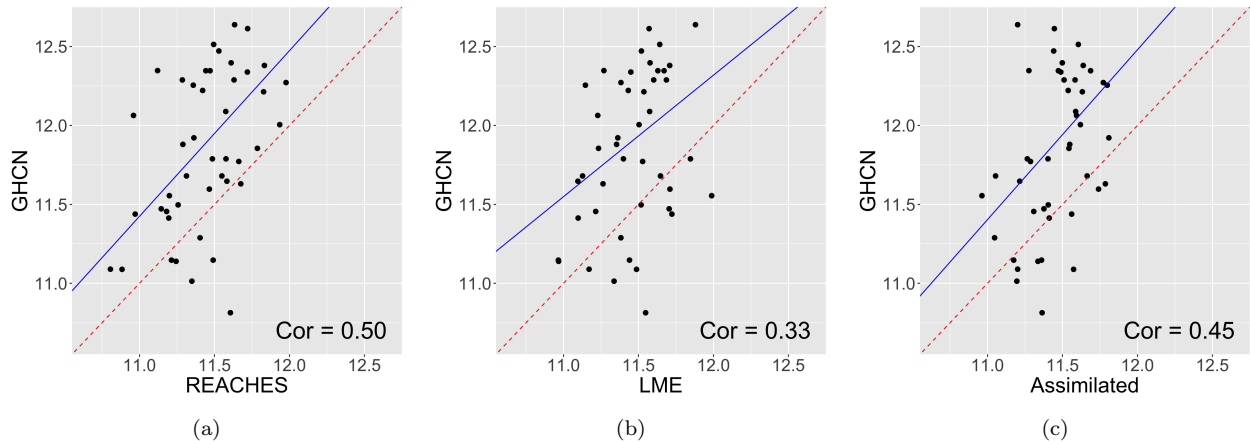


Figure 13: Scatter plots of Beijing temperatures from 1861 to 1911: (a) GHCN vs. Celsius-scale REACHES; (b) GHCN vs. LME; (c) GHCN vs. Assimilated.

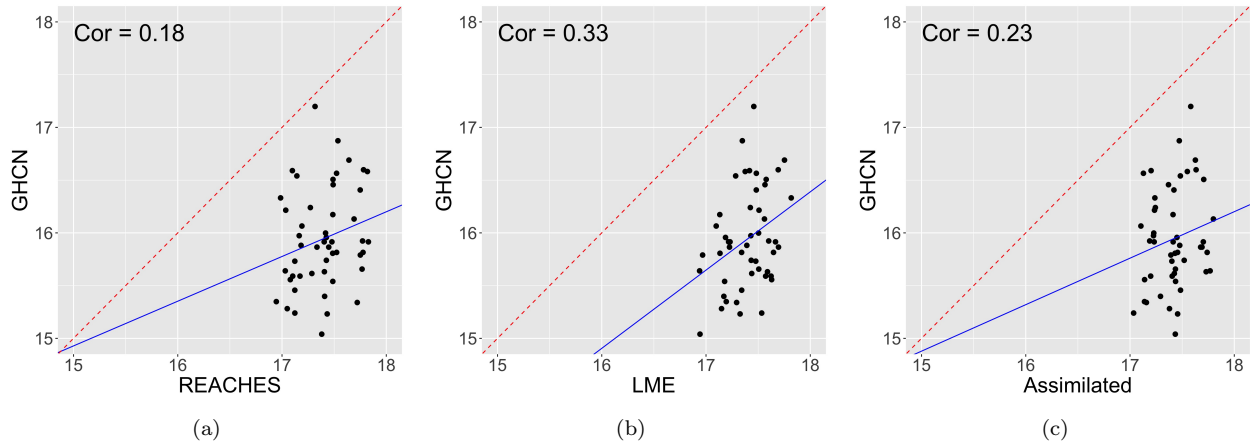


Figure 14: Scatter plots of Shanghai temperatures from 1857 to 1911: (a) GHCN vs. Celsius-scale REACHES; (b) GHCN vs. LME; (c) GHCN vs. Assimilated.

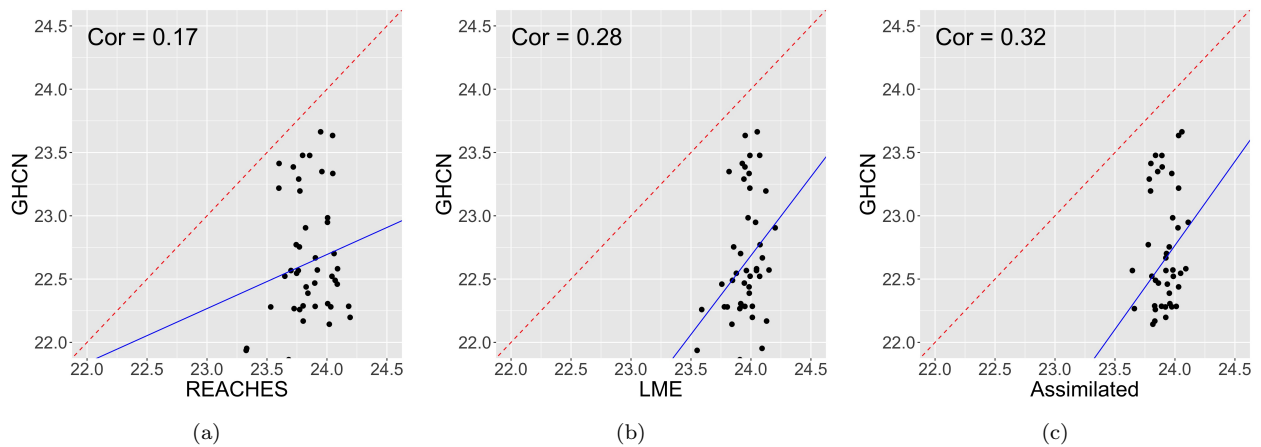


Figure 15: Scatter plots of Hong Kong temperatures from 1853 to 1911: (a) GHCN vs. Celsius-scale REACHES; (b) GHCN vs. LME; (c) GHCN vs. Assimilated.

broader regional trends.

While the Celsius-transformed REACHES predictions outperform the LME simulation outputs in Beijing in terms of correlation coefficients, they do not perform as well in Shanghai and Hong Kong. Our Bayesian assimilated predictions, however, further integrate information from the LME simulations, resulting in improved performance in Shanghai and Hong Kong. Specifically, compared to the Celsius-transformed REACHES predictions, our Bayesian assimilation method increases the correlation coefficient from 0.18 to 0.23 in Shanghai and 0.17 to 0.32 in Hong Kong. However, it decreases slightly from 0.50 to 0.45 in Beijing. Despite the slight decrease in Beijing, the correlation remains high, underscoring the robustness of our method. The overall improvement in correlation in Shanghai and Hong Kong confirms the effectiveness of integrating historical proxy data with climate model simulations, particularly in regions where individual methods perform less effectively.

The higher correlation in Beijing compared to Shanghai and Hong Kong may be attributed to several factors. One possibility is that the historical records from Beijing contain more climate-relevant details or are more directly influenced by large-scale climatic patterns, making them more reflective of the temperature variations captured in the GHCN records. Additionally, Beijing’s inland continental climate might exhibit temperature variations that are more pronounced and thus more accurately recorded in historical documents. In contrast, the coastal climates of Shanghai and Hong Kong may be influenced by local factors that are less consistently documented.

For periods preceding the GHCN instrumental records, we rely on comparisons with documented historical climate events. During the late Ming dynasty in the 17th century, historical records describe a period of significant cooling, often associated with the Little Ice Age, a global climatic interval characterized by cooler temperatures between the 14th and 19th centuries. This cooling trend is believed to have profoundly impacted agriculture and society in China, contributing to social unrest and the eventual decline of the Ming dynasty. As depicted in Figure 12, our predicted temperatures capture this cooling trend

during the late Ming period, demonstrating a pronounced temperature decrease consistent with historical accounts. This correspondence reinforces the credibility of our predictions for earlier centuries and underscores the effectiveness of our data assimilation approach in reconstructing long-term climate variability.

By integrating qualitative historical records with quantitative climate model simulations, our method provides a more comprehensive understanding of past climate variability in China. The ability to accurately reconstruct temperature variations during the Ming and Qing dynasties validates our approach and highlights its potential for contributing valuable insights into historical climatology and the broader field of paleoclimatology.

## 6. Discussion and Conclusions

In this article, we presented a comprehensive Bayesian data assimilation framework to reconstruct historical temperatures in China during the Ming and Qing dynasties. Our approach integrates ordinal-scale temperature indices from the REACHES dataset with climate model simulations from the LME. We converted the ordinal-scale REACHES indices into Celsius units using quantile mapping, facilitating direct comparisons with instrumental records and climate model simulations.

A key component of our methodology is the use of kriging based on a zero-mean Gaussian process that accounts for data missing not at random. This geostatistical approach allows us to generate spatially continuous temperature estimates across East China, extending beyond the specific locations of the original observations. Unlike previous methods, which are often confined to predefined subregions, our approach enables temperature reconstruction at any point location within the study area. This is a significant advancement over existing methods, such as those presented by Wang et al. (2024), who reconstructed temperature indices restricted to 15 subregional domains in China using the REACHES dataset.

We developed a nonstationary time series prior model within our Bayesian framework, leveraging LME climate simulations to estimate model parameters. Our approach involved regularized maximum likelihood estimation with a fused lasso penalty, which enforced spar-

sity and encouraged temporal smoothness in the parameter estimates. This method allowed us to effectively incorporate information from the LME data as our temperature prior.

A key aspect of our methodology was assimilating Celsius-transformed REACHES data using the Kalman filter and smoother algorithms. This systematic method updated and corrected temperature estimates based on Celsius-scale REACHES data and model simulation outputs. Our data assimilation method demonstrated significant improvements in the correlation of temperature estimates with the GHCN instrumental records, enhancing the reliability of historical climate reconstructions.

The successful application of our method to major cities demonstrates its potential for reconstructing temperature variations across East China. By generating spatially continuous temperature estimates, we can extend our analysis to any point location within the region, a capability not offered by previous methods. This flexibility is particularly valuable for studying historical climate variations in areas with sparse or unevenly distributed data.

In comparison to recent work by Wang et al. (2024), who reconstructed temperature indices using the REACHES database but did not transform the indices into Celsius scales, did not consider data assimilation, and was limited to 15 subregional domains, our approach offers a more flexible and comprehensive framework. By utilizing kriging and Bayesian data assimilation, we can generate temperature estimates at any location within East China, providing finer spatial resolution for studying localized climate patterns.

While promising, our approach does encounter limitations, particularly concerning the quality and completeness of the REACHES dataset, which can vary significantly across regions and periods. For example, the discrepancy noted in Shanghai underscores the need for higher-quality input data. Future efforts to digitize and standardize more historical documents could substantially improve data quality and coverage.

Further research might explore the sensitivity of our results to different prior models and incorporate additional proxy data types to enhance the robustness of our reconstructions. Additionally, we could investigate the application of more advanced data assimilation tech-

niques, such as particle filters or ensemble Kalman filters, which may offer better handling of non-linearities and non-Gaussian uncertainties inherent in climate data.

In conclusion, our study not only demonstrates the feasibility of using Bayesian data assimilation to reconstruct historical temperatures but also highlights the potential for extending this approach to a broader range of locations, thereby providing a more detailed and comprehensive understanding of historical climate patterns across East China.

## References

- Brousseau, P., Berre, L., Bouttier, F., and Desroziers, G. (2011). Background-error covariances for a convective-scale data-assimilation system: Arome–france 3d-var. *Quarterly Journal of the Royal Meteorological Society*, 137(655):409–422.
- Brönnimann, S., Allan, R., Ashcroft, L., Baer, S., Barriendos, M., Brázdil, R., and et al. (2019). Unlocking pre-1850 instrumental meteorological records: A global inventory. *Bulletin of the American Meteorological Society*, 100(12):ES389 – ES413.
- Cannon, A. J., Sobie, S. R., and Murdock, T. Q. (2015). Bias correction of gcm precipitation by quantile mapping: How well do methods preserve changes in quantiles and extremes? *Journal of Climate*, 28(17):6938 – 6959.
- Cleveland, W. S. (1979). Robust locally weighted regression and smoothing scatterplots. *Journal of the American Statistical Association*, 74(368):829–836.
- Cressie, N. (1985). Fitting variogram models by weighted least squares. *Journal of the International Association for Mathematical Geology*, 17(5):563–586.
- Cressie, N. (1993). *Statistics for Spatial Data*, chapter 3, pages 105–118. John Wiley & Sons, Ltd.
- Evensen, G. (2009). The ensemble kalman filter for combined state and parameter estimation. *IEEE Control Systems Magazine*, 29:83–104.

- Fan, K.-w. (2023). The little ice age and the fall of the ming dynasty: A review. *Climate*, 11(3).
- Genz, A. and Bretz, F. (2009). *Computation of Multivariate Normal and t Probabilities*, volume 195 of *Lecture Notes in Statistics*. Springer.
- Goeman, J. (2022). L1 penalized estimation in the cox proportional hazards model. *Biometrical Journal*, 52(1):70–84.
- Goosse, H., Guiot, J., Mann, M. E., Dubinkina, S., and Sallaz-Damaz, Y. (2012). The medieval climate anomaly in europe: Comparison of the summer and annual mean signals in two reconstructions and in simulations with data assimilation. *Global and Planetary Change*, 84-85:35–47. Perspectives on Climate in Medieval Time.
- Jones, P. D. and Mann, M. E. (2004). Climate over past millennia. *Reviews of Geophysics*, 42(2).
- Kalman, R. E. (1960). A New Approach to Linear Filtering and Prediction Problems. *Journal of Basic Engineering*, 82(1):35–45.
- Kalnay, E. (2002). *Atmospheric Modeling, Data Assimilation and Predictability*. Cambridge University Press.
- Oke, P. R., Allen, J. S., Miller, R. N., Egbert, G. D., and Kosro, P. M. (2002). Assimilation of surface velocity data into a primitive equation coastal ocean model. *Journal of Geophysical Research: Oceans*, 107(C9):5–1–5–25.
- Otto-Bliesner, B. L., Brady, E. C., Fasullo, J., Jahn, A., Landrum, L., Stevenson, S., Rosenbloom, N., Mai, A., and Strand, G. (2016). Climate variability and change since 850 ce: An ensemble approach with the community earth system model. *Bulletin of the American Meteorological Society*, 97(5):735 – 754.

- Tibshirani, R., Saunders, M., Rosset, S., Zhu, J., and Knight, K. (2004). Sparsity and Smoothness Via the Fused Lasso. *Journal of the Royal Statistical Society Series B: Statistical Methodology*, 67(1):91–108.
- Tsay, R. S. (2005). *Analysis of financial time series*. John wiley & sons.
- Wang, P.-K., Lin, K.-H. E., Liao, Y.-C., Liao, H.-M., Lin, Y.-S., Hsu, C.-T., Hsu, S.-M., Wan, C.-W., Lee, S.-Y., Fan, I.-C., Tan, P.-H., and Ting, T.-T. (2018). Construction of the reaches climate database based on historical documents of china. *Scientific Data*, 5.
- Wang, P. K., Lin, K.-H. E., Lin, Y.-S., Lin, H.-J., Pai, P.-L., Tseng, W.-L., Huang, H.-C., and Lee, C.-R. (2024). Reconstruction of the temperature index series of china in 1368–1911 based on REACHES database. *Scientific Data*, 11:1117.
- Wang, Z., Gladwin, D. T., Smith, M. J., and Haass, S. (2021). Practical state estimation using kalman filter methods for large-scale battery systems. *Applied Energy*, 294:117022.
- Wikle, C. K. and Berliner, L. M. (2007). A bayesian tutorial for data assimilation. *Physica D: Nonlinear Phenomena*, 230:1–16.
- Zheng, J., Xiao, L., Fang, X., Hao, Z., Ge, Q., and Li, B. (2014). How climate change impacted the collapse of the ming dynasty. *Climate Change*, 127:169–182.